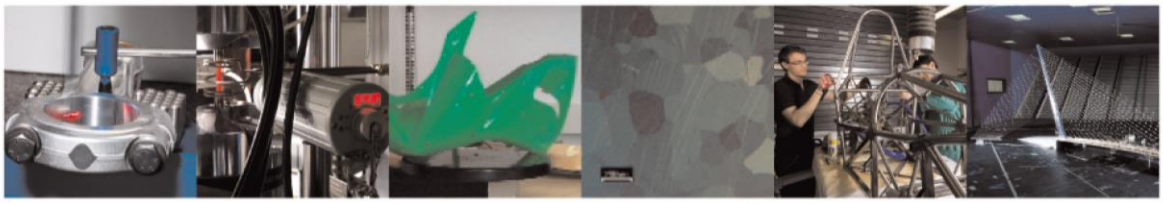

Using recycled material to produce gas-atomized metal powders for additive manufacturing processes

S. Cacace, V. Furlan, R. Sorci, Q. Semeraro, M. Boccadoro

This is a post-peer-review, pre-copyedit version of an article published in Journal of Cleaner Production. The final authenticated version is available online at:
http://dx.doi.org/10.1016/j.jclepro.2020.122218

DIPARTIMENTO DI MECCANICA ■ POLITECNICO DI MILANO
via G. La Masa, 1 ■ 20156 Milano ■ EMAIL (PEC): pecmecc@cert.polimi.it
http://www.mecc.polimi.it
Rev. 0

WORDCOUNT: 9207

Using recycled material to produce gas-atomized metal powders for additive manufacturing processes

Authors: S. Cacace[a*], V. Furlan[a], R. Sorci[b], Q. Semeraro[a], M. Boccadoro[c]

[a] Dipartimento di Ingegneria Meccanica, Politecnico di Milano, Via La Masa 1, 20156 Milano, Italy

[b] Rina Consulting, Centro Sviluppo Materiali S.p.A., Via di Castel Romano 100, 00128 Roma, Italy

[c] Tenova S.p.A., Via Gerenzano 58, 21053 Castellanza, Italy

[*] corresponding author e-mail address: stefania.cacace@polimi.it

Abbreviations[1]:

[1]AM: Additive Manufacturing; El: Elongation after fracture (%); LMD: Laser Metal Deposition; PSD: Particle Size Distribution; SLM: Selective Laser Melting; UTS: Ultimate Tensile Strength (MPa); VIGA: Vacuum Induced Gas Atomization; YS: Yield Strength (MPa)

Abstract

Additive manufacturing refers to the technologies used to directly produce parts from a three-dimensional model. Recycled AISI 316L and standard AISI 316L materials were used to produce powders via gas atomization process, and two additive manufacturing technologies, i.e., selective laser melting and laser metal deposition, were investigated. This study aims to determine the feasibility of using recycled material to produce powders for additive manufacturing. For each technology, the effect of process parameters on the solidification of the recycled powders was evaluated. Then, tensile tests were conducted on the specimens produced using the optimized process parameters. Specimens from both the technologies exhibited higher ultimate tensile strength values than standard AISI 316L. Recycled powders made from selective laser melting and laser metal deposition exhibited tensile strength values of 653 ± 1.79 MPa and 675 ± 2 MPa, respectively, whereas the standard powders exhibited a tensile strength of 594 ± 0.89 and 585 ± 3.1 MPa, respectively. We conclude that recycled AISI 316L can be used to produce powders for AM applications, resulting in good processability and high mechanical properties.

Keywords: additive manufacturing; sustainability; stainless steel; tensile strength

1. Introduction

Additive manufacturing (AM) technologies enable the creation of 3D parts layer by layer. In industrial manufacturing, AM has become a feasible means of production in sectors such as aerospace and biomedical manufacturing.

Selective laser melting (SLM) and laser metal deposition (LMD) technologies use powders whose properties determine the stability and robustness of the two processes. These technologies have been receiving increasing amounts of attention by the scientific community, as reviewed by Vock et al. (2019).

The SLM process starts with powder material being spread by a roller on a build plate, resulting in a homogeneous layer. A laser source selectively scans and melts the thin powder layer according to the part cross-section based on the 3D digital part model. The building chamber is filled with inert gas, resulting in an

atmosphere with a low oxygen content during building. The molten powder solidifies forming a solid layer of the part. When the scanning of the layer is completed, the building platform is lowered by a predefined quantity (i.e. the layer thickness) and the process is repeated until the part is completed. In the LMD process, the parts are produced layer by layer starting from the 3D digital model of the part (as in SLM). In LMD, the part is produced by injecting the metal powder directly on the melt pool through a deposition head, which also conveys the laser. The powder is controlled by a powder feeder and it is delivered up to the deposition head with a carrier gas. The deposition head is mounted on an anthropomorphic robot, or a cartesian axis and its movement allows the layer-wise production of complex parts. Differently from SLM, in LMD the powder and laser are applied simultaneously. LMD and SLM are among the most common powder-based AM technologies, see for example Tofail et al. (2018), and their applications are in the automotive, aerospace sectors. Schematics of both SLM and LMD are showed in Figure 1.

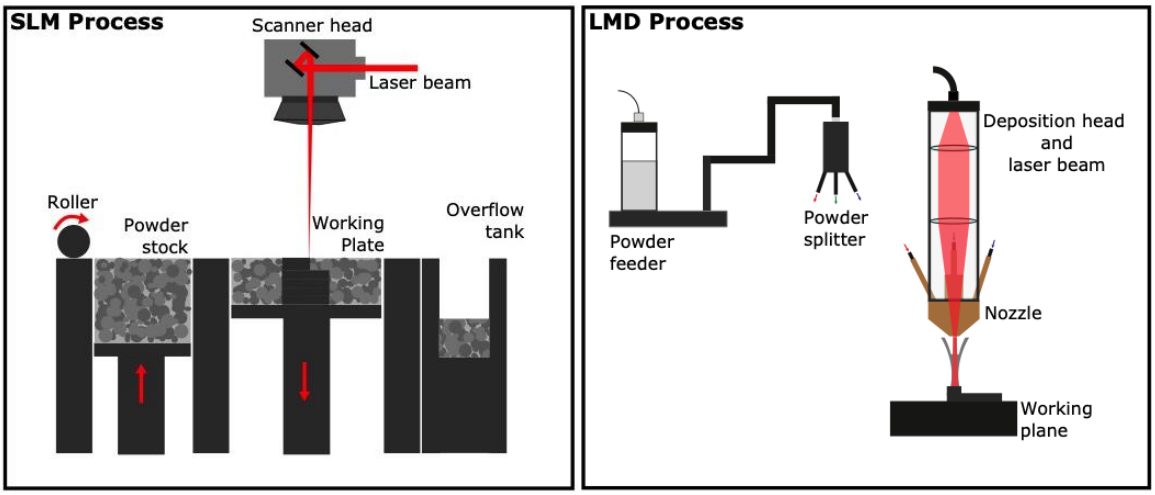

Fig. 1 – Schematic representation of SLM and LMD processes

Both processes involve the use of powder which properties can affect the performance of 3D parts. In this perspective, the objective of this study is to use powder coming from scrap material to produce additively manufactured parts using SLM and LMD processes. The use of powder from recycled material has two main advantages: the first one is in terms of sustainability of the AM processes, the second is in terms of cost of the powders. These two aspects will be debated later in the Introduction. The use of non-standard powders needs to be studied carefully, as it is known from the literature that small deviations from nominal chemical composition might have a strong impact on the processability of the powders and on the final part properties.

The ability of powders to be processed is commonly defined *processability*. A powder has good processability if it can be successfully melted to generate a 3D part with low porosity and defects. For this reason, it is important to perform extensive experimental campaigns to study the possibility to use these new powders for SLM and LMD processes.

A state of the art on the influence of the powder chemical composition on the processability of powders in SLM and LMD is hereby proposed. Kakinuma et al. (2016) and Khayat and Palmer (2018) used different batches of a nickel-chromium superalloy (Inconel 625) in the LMD process. Khayat and Palmer (2018) found that using a range of Fe composition from 1% wt to 4% wt the resulting mechanical properties did change. The low content of Fe in the powders resulted in higher strength and lower elongation. Kakinuma et al. (2016) found that Si and C contents of the batches influence the manufactured part properties; a higher content of Si was correlated with higher porosity.

Tomus et al. (2017) used two different Hastelloy X (a nickel-based superalloy) powders differing slightly in their Si, Mn, and C contents and they found that low levels of Si and C improve the solidification process of AM. Engeli et al. (2016) studied 7 batches of a gas atomized nickel-chromium based superalloy (Inconel 718) processed with an industrial SLM system. In this case, the Si content had a strong impact on the part crack susceptibility. Based on these previous studies, we conclude that even small variations in the chemical composition of the powders may affect the processability of the powders and consequently the quality of the finished product. Also, the previous studies did not employ stainless steel powders or recycled material for the atomization process.

The influence of the powder on the properties of the 3D printed part, when using powder-based AM technologies, has not been studied extensively. This is because end-users of powder-based AM technology tend to use the powder supplied by the machine manufacturer, as the optimal processing parameters of these powders are provided. Moreover, few alloys are available for powder-based AM processes applied to traditional machining (Sames et al., 2016). For these reasons, the literature on the influence of variations in the chemical composition of powder feedstock on 3D-printed final part properties is limited. Overall, there is a lack of knowledge on the relationship between powder properties and the 3D printed final part. This lack of information implies that the use of powders produced using a non-standard method is not straightforward and it is not possible to compare the new research results with previous literature data.

The importance of powder production is relevant not only to the 3D printed part, but also to the sustainability of the process. AM is known to reduce material waste and to increase energy efficiency, as shown by Huang et al. (2013) and Chen et al. (2015). The former compared the sustainability of AM to traditional processes. Chen et al. (2015) suggested that AM technologies improve energy efficiency due to the optimization of the design process and supply chain. Sreenivasan et al. (2010) pointed out that to assess sustainability, the analysis cannot be limited to the AM process by itself, but should consider the overall value chain, including refurbishment and remanufacturing, as suggested by Rejeski et al. (2018).

Ford and Despeisse (2016) reported that AM materials are not greener as compared to those used for traditional manufacturing. This is especially true for metal-based AM technologies that use metal powders produced via atomization (generally gas atomization, although water and plasma atomization are also viable options).

Consequently, there is a growing interest in using greener materials for AM production, which includes powder-based AM technologies. Fullenwider et al. (2019) used ball milling on 304L stainless steel machining chips to produce powders for the LENS® process (an AM technology similar to LMD) and successfully produced single tracks using ball-milled swarf as powder material. However, they did not produce 3D samples to test other mechanical properties.

If the processability and mechanical properties of the recycled powder are comparable with the standard material, then new opportunities for powder manufacturers will be available, along with other economic advantages. Feedstock cost is one of the barriers preventing the wider diffusion of AM technologies (Niaki et al., 2019). In breaking down the cost of a reference part, Lindemann et al. (2012) found that the cost of the material constitutes up to 11 % of the overall batch cost (190 parts). The authors also provide information about cost structure, which is dependent on these four drivers: the building rate, utilization rate, powder cost, and machine investment. In most cases, the material cost accounts for approximately 10% of the production cost. In a cost analysis of the AM process, Baumers et al. (2017) estimated that the material accounts for 10% of the AM production cost. The use of recycled metal in the atomization process does not require incremental costs of setup, and therefore it does not impact on the final cost of the material. At the present stage, feedstock material for AM is only produced from virgin metal and its cost is consequently higher. In case the processability of the recycled powders is verified, AM end-users could choose the material feedstock quality which meets their requirements also considering low-cost recycled powders.

Therefore, alternative methods of producing feedstock material for powder-based AM technologies is of great interest owing to two reasons, i.e., sustainability and cost. This works aims to study the possibility of producing atomized metal powders from recycled material at the atomization stage. To the best of our knowledge, the use of recycled material for metal powder production in AM has not been previously reported. Moreover, this is one of the few works available in the literature that compares directly SLM and LMD processes. In this study, we used recycled metal as a raw material in the atomization process and the resulting powders are then employed in SLM and LMD. To accomplish our aim, three different stainless-steel powders (AISI 316L), atomized via vacuum inert gas atomization (VIGA), were produced starting from three ingots: one ingot was produced with standard material whereas the other two powders were obtained from recycled material. The two AISI 316L powders produced from recycled metal, were used to produce specimens via LMD and SLM, and the mechanical properties of the resulting specimens were compared with those of the standard material.

2 Material and Methods

2.1 Workflow

We used three batches of stainless steel 316L powders, with each powder divided into two particle size distributions: a fine fraction (15-60 μm) for the SLM process and a coarse fraction (45-120 μm) for the LMD process. Powders were characterized in terms of particle size distribution (PSD), chemical composition, and flowability. The objective was to compare the properties of the final 3D printed part made from two recycled powders to those of the standard material.

The workflow for both processes were similar. First, the process parameters that maximize the density of the final 3D printed part were selected. It should be noted that the parameters involved are different for each technology. The best processing conditions were used to produce tensile specimens for all three powder batches via SLM and LMD. The complete workflow is shown in Figure 2.

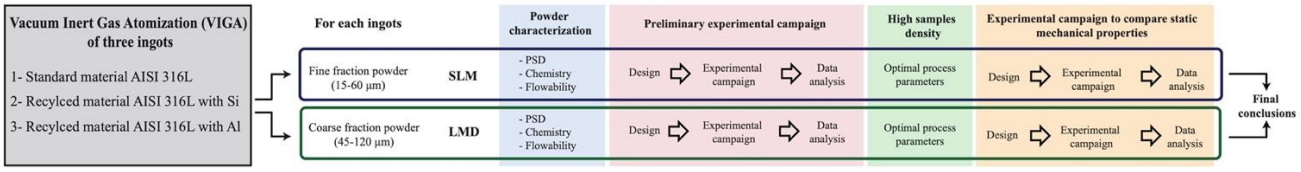

Fig 2. Study workflow

2.2 Powder characterization

The powders used for the investigation were produced by a Vacuum Induced Gas Atomization (VIGA) pilot plant named RINA CSM (RINA Consulting Centro Sviluppo Materiali, Italy). In the VIGA process, vacuum induction melting is used to melt the material. The molten metal is then poured from an insulated tundish through a nozzle to form a thin stream of material that is disintegrated into droplets by high-pressure inert gas jets, Popovich and Sufiiarov (2016).

Three different ingots (batches) of AISI 316L were used for atomization. The first is a standard AISI 316L ingot whereas the second and third batches of powders were obtained by using AISI 316L scrap material produced by a deoxidizing process with the addition of Si and Al, respectively. From each ingot, two particle size distributions (PSD) were obtained through a sieving process. One distribution was designed for the SLM process, between 15–60 μm, while the second was designed for the LMD process (between 45–120 μm). These are the standard distributions used for the two processes according to the literature and the industrial practice, Sames et al. (2016), Tan et al. (2017). The atomization process was optimized to produce powders in the range 15-60 μm, thus the SLM process produced 5 kg of each powder while the LMD process produced only 2 kg of powder after sieving.

The nomenclature of the powders used during the study is reported in Table 1. Powders were characterized in terms of apparent density (ISO 3923) and flowability (ASTM B213 and ASTM B417). Particle size distribution was measured using a Malvern Mastersizer 2000, according to standard ISO 13320:2009. Based on the machine manufacturer, the reproducibility of the PSD measurement is 1% while the repeatability is 0.6%. Of course, these values strongly depend on how the sample was prepared and segregation could have an impact when measuring powders higher than 50 μm. In our case, the sampling was carried out following the standard procedures indicated in UNI EN ISO 14284:2004, so it is fair to assume that the reproducibility error is close to 1%. Nitrogen and oxygen contents were measured using a LECO CS600 and LECO O-N TCH 600, respectively, following standard protocols (ASTM E1019-11). Sampling procedures also followed standard protocols (UNI EN ISO 14284:2004). Si and Al were measured using X-ray fluorescence according to ASTM E572-02a using a Philips Panalytical Magix Pro PW 2440 Spectrometer. XRF measurement were performed

on the powders before sieving, thus each powder batch was analysed only once. The use of XRF method for bulk material analysis and chemical characterization of AM powders is commonly used (Cooke and Slotwinski, 2012).

Table 1. Nomenclature of the powders investigated in this study

Process	Powder	Nomenclature
SLM	Standard AISI 316L	1-SLM
	Industrial AISI 316L–Si	2-SLM
	Industrial AISI 316L–Al	3-SLM
LMD	Standard AISI 316L	1.LMD
	Industrial AISI 316L–Si	2-LMD
	Industrial AISI 316L–Al	3-LMD

2.3 SLM Experimental Plan

SLM samples were produced using the Renishaw AM250 industrial system. The machine is equipped with a 200 W fibre laser producing a laser spot of approximately 70 μm at the focal position. As Renishaw AM250 functions in pulsed wave mode, the process parameters defining the laser speed are exposure time and point distance (Figure 3). Exposure time, t, is the duration of a single laser pulse; point distance, d_p, is the distance between two consecutive laser spots; and hatch distance, d_h, is the distance between two consecutive scanning lines. Before processing, vacuum is applied to the building area to reach an oxygen content lower than 1000 ppm; during the process, the chamber is filled with a constant flow of argon. The substrate material was an AISI 316L stainless steel plate. The reduced build volume (RBV) system provided by Renishaw was used to produce all the samples. The RBV system allows for the reduction of the building volume as well as the easy exchange of powders for experimental purposes. This flexibility is coupled with all the advantages of an industrial system (i.e. laser type, atmospheric control).

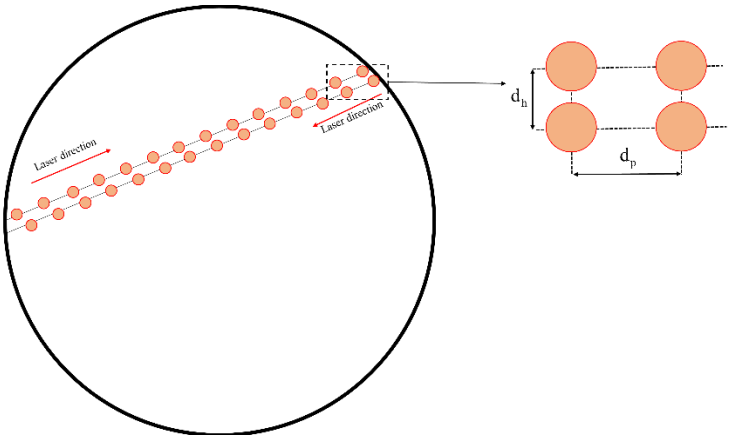

Fig 3. Example laser path on a layer where the point distance and hatch distance are defined

2.3.1 SLM: exploratory experiments

In the preliminary experiments, specimens were designed with a cylindrical shape (5 mm diameter and 12 mm height). The density of 3D printed parts was measured using an electronic scale (Precisa 100A-300M) with a density measurement kit using a standard procedure (ASTM B962-17).

The objective was to identify the combination of process parameters that ensures the highest density. As the optimal process parameters for the standard AISI 316L powder are known, only powders 2-SLM and 3-SLM were considered in this stage. The preliminary experiment is required because differences in the chemical compositions of 2-SLM and 3-SLM powders may affect the processability window, i.e. the range of parameter values in which high density is achieved.

Laser power was applied at its highest value (200 W) constantly to increase productivity. The experiment used a factorial design with the following factors: exposure time t (µs), hatch distance d_h (µm), and point distance d_p (µm). The list of factors and fixed parameters used to evaluate the final 3D printed part density are shown in Table 2.

Table 2. Fixed parameters and factors used for experiments investigating SLM part density

Fixed parameters		**Factors**	
Power	200 W	Exposure time, t	64–96 µs
Focus distance	0 mm	Point distance, d_p	48–72 µm

Layer thickness	0.05 mm	Hatch distance, d_h	80–120 µm

The experimental design was a 2^3 factorial design involving t, d_p, and d_h and with a centre point. Experiments on both deoxidized AISI 316L powders used the same experimental design. The centre point of the design (Table 3) was the suggested processing condition for standard AISI 316L by the SLM machine manufacturer.

Using the conditions in Table 3, the expected final 3D printed part density should be higher than 7.9 g/cm^3 (i.e. higher than 99% of the bulk density of AISI 316L). The factorial points of the design were selected within ± 20% of the centre point (Table 4). All three process parameters can be combined to determine the amount of energy per unit surface delivered to the powder during the process; this index is called Energy Density E_d. The relationship between SLM final part density and energy density is well-known and, as shown by Cherry et al. (2015), it can be used to describe the solidification process of SLM parts. Energy density is closely related to the process quality: energy should be high enough to completely melt the powders but not excessively high, as in this case the molten material is subjected to turbulent flow causing the formation of porosity during the melting phase. The energy density (J/cm^2) for pulsed lasers is defined as (Demir et al., 2017):

$$E_d = \frac{P \cdot t}{d_p \cdot d_h} \ \text{J/cm}^2 \qquad (1)$$

The factorial design was replicated two times while the centre point was replicated 6 times. Summing up, for each powder, the number of samples for density evaluation were: 2^3x2+6=22. The centre point was replicated six times, instead of the usual three replicates, because this condition was used as a control treatment for the Dunnet comparison test, as suggested by Montgomery (2017).

Table 3. Suggested parameters reported by Renishaw for AISI 316L

Power (W)	t (µs)	d_p (µm)	d_h (µm)
200	80	60	100

Table 4. 2^3 factorial design for SLM experiment

Treatment	**P [W]**	**t [µs]**	**dp [µm]**	**dh [µm]**	**E_d [J/cm^2]**

1	200	64	48	80	333
2	200	96	48	80	500
3	200	64	72	80	222
4	200	96	72	80	333
5	200	64	48	120	222
6	200	96	48	120	333
7	200	64	72	120	148
8	200	96	72	120	222
9 (Centre point)	200	80	60	100	267

2.3.2 SLM: tensile properties experiments

The tensile properties of all three powders were evaluated. Five samples were produced for each powder and ultimate tensile strength (UTS), yield strength (YS), and Young modulus and elongation after fracture (El %), were evaluated. Tensile tests were performed using an MTS Alliance RF/100 machine according to ASTM E8-16 standards. Tensile specimen geometry specifications are reported in Table 5.

Table 5. Specimen geometry for tensile tests of the SLM process [mm]

Dimension, mm, for test Specimen with Gauge Length four times the Diameter [ASTM E8]	
G: Gauge length	16.0 ± 0.1
D: Diameter	4.0 ± 0.1
R: Radius of fillet, min	4
A: Length of reduced section, min	20

The number of specimens for tensile strength characterization was determined to calculate the power of a One-Way ANOVA with three levels. Five replicated samples allowed a ±10% probability of not detecting an existing difference in UTS equal to 55 MPa between different powders. To evaluate the power of the test, the

level of variability of the UTS was estimated based on previous experiments (σ=20 MPa). The reference UTS value for standard AISI 316L is 550 MPa.

For standard AISI 316L powders (SLM-1) (Treatment 9), we followed the processing conditions recommended by the machine manufacturer reported in Table 3. We used the same combination for 2-SLM and 3-SLM powders.

Tensile specimens were built to assume a near net shape; the SLM system and the sample head was threaded before testing.

2.4 LMD Experimental Plan

The LMD system comprises a fibre laser IPG Photonics (YLS 3000) with a laser wavelength of 1070 nm and a maximum power of 3 kW. The beam is delivered by a 50-µm feeding fibre coupled with a 400-µm process fibre by a fibre-to-fibre coupler. The deposition head (Kuka Industries MWO-I-Powder) is equipped with a 129-mm collimation lens and a 200-mm focal lens. The collimation lens is adjustable to various positions to obtain different spot dimensions at the target plane. In the present work, the collimation lens was maintained in a fixed position resulting in a spot diameter of 1.2 mm on the substrate. The deposition head is mounted on a 6-axis anthropomorphic robot (ABB IRB 4600-45) equipped with a 3-way nozzle (3-JET-SO16-S, Fraunhofer ILT) for powder deposition (Figure 4). The powder flow is controlled by a powder feeder (TWIN PF 2/2-MF, GTV). A carrier gas is used to deliver the powder from the powder feeder through the powder splitter up to the 3-way nozzle. Argon is used both as a carrier and shielding gas during the process. The substrate material was an AISI 316L 5-mm-thick ingot.

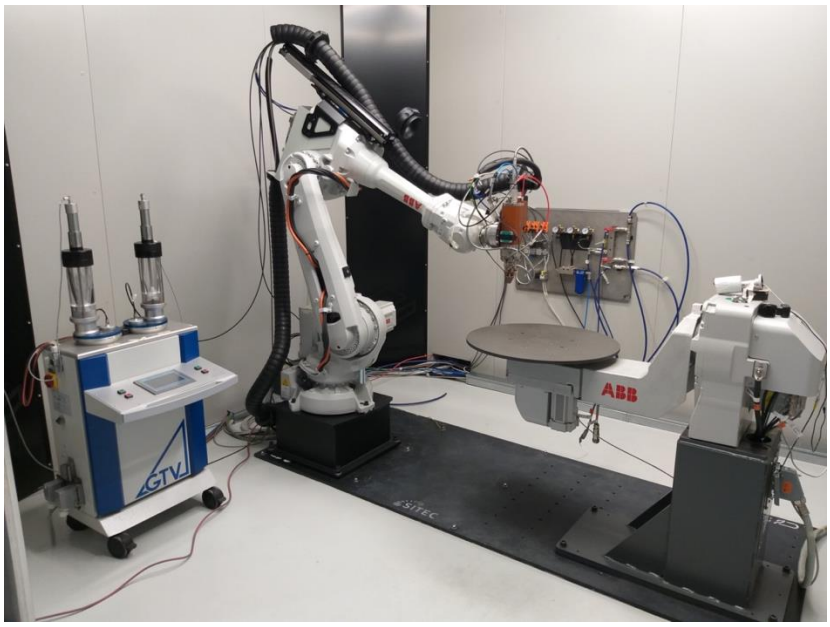

Fig 4. The LMD system

2.4.1 LMD: exploratory experiments

In the preliminary experiments for density evaluation, the specimens were printed as cubes with dimensions 10 x 10 x 10 mm^3. Samples were obtained using an alternate bi-directional strategy with a 45% tracks overlap (Figure 5).

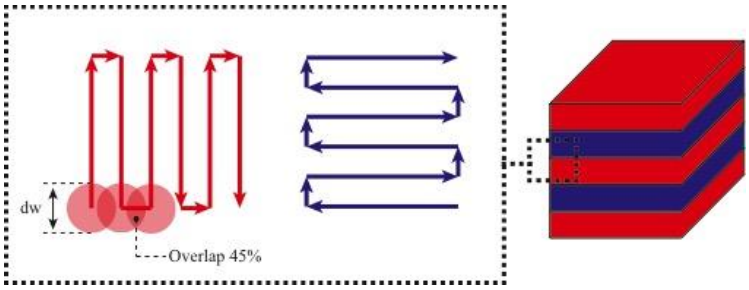

Fig 5. Schematic representation of LMD strategy

Part density was measured as described in Section 2.3.1 for SLM specimens.

Process parameters were varied to identify the best processing conditions in terms of final 3D printed part density produced from the recycled powders, as their processability cannot be ensured due to the differences in chemical composition. The factors considered were laser power P (W) and the powder flow rate g (g/min). A list of the parameters and factors considered is shown in Table 6.

Table 6. Fixed parameters and factors of LMD experiments

Fixed parameters		F**actors**	
Speed	30 mm/s	Power, P	370 - 470 W
Robot height increment	0.2 mm	Powder flow rate, g	8 - 10.3 g/min
Stand-off distance	12 mm		
Laser spot diameter	1.2 mm		
Track overlap	45%		
Shielding gas flow rate	25 l/min		
Carrier gas flow rate	7.5 l/min		

The experiment followed a 3^2 factorial design with experimental conditions listed in Table 7. Experiments on both industrial AISI 316L powders followed the same design with no replicates. Therefore, the total number of samples evaluated for density was 3^2=9 for 2-LMD and 3-LMD. The number of samples produced for LMD was significantly less than that used for SLM because of the limited amount of powder available. As already discussed in section 2.2, the atomization process was implemented to produce powders with particle sizes in the SLM range; the LMD fraction was obtained by sieving.

The reference conditions used for LMD experiments were based on previous investigations on the standard material, AISI 316L. The process parameters of the reference conditions for standard AISI 316L powders undergoing the LMD process are reported in Table 8, which also comprises treatment 5 in Table 7.

The results of the preliminary experiments identified the parameters that maximize the density of the specimens and were then selected for the experiments comparing the static properties of the three powders.

Table 7. 3^2 factorial design for LMD experiments

Treatment	P [W]	g [g/min]
1	370	8
2	370	9.2

3	370	10.3
4	420	8
5	420	9.2
6	420	10.3
7	470	8
8	470	9.2
9	470	10.3

Table 8. Reference condition for AISI 316L undergoing the LMD process

P [W]	v [mm/s]	g [g/min]	Δz [mm]	Sod [mm]	d_t [mm]	overlap [%]
420	30	9.2	0.2	12	0.9	45

2.4.2 LMD: tensile properties experiments

The specimen geometry of LMD powders for tensile tests was selected according to ASTM E8. The main characteristics of the specimens tested for tensile strength are reported in Table 9. Samples were obtained by cutting the desired shape using electrical discharge machining (EDM). Tensile tests were performed using a MTS Alliance RF/100 machine. Tests were conducted on unthreaded samples; instead, pneumatic grips were used. UTS, YS, and El were considered as responses

Table 9. Specimen geometry for tensile tests according to ASTM E8, [mm]

Dimension, mm, for test specimens with reduced size [ASTM E8]	
G: Gauge length	25.0 ± 0.1
W: Width	6.0 ± 0.1
T: Thickness max	≤6
R: Radius of fillet, min	6
L: Overall length, min	100
A: Length of reduced parallel section, min	32

B: Length of grip section, min	30

Due to lack of powder, only three tensile samples were produced for each batch. In this case, considering a standard deviation of the process equal to 20 MPa and a difference of interest of 55 MPa, the power of the test is equal to 60%.

3 Experimental results

3.1 Morphological and chemical analyses of powders

For SLM and LMD processes, powders are usually characterized in terms of Particle Size Distribution (PSD), shape and flowability. The PSD should belong to pre-defined intervals depending on the process in which they are used. For SLM, the standard range is 15-60 μm, for LMD 45-120 μm. The shape should be close to a spherical one with a smooth surface, to improve flowability and reduce friction between particles as they are spread on the build platform (SLM) or carried in the deposition head (LMD). Flowability indicates how well a powder flows, a higher flowability is desired in both SLM and LMD processes.

The Particle Size Distribution (PSD) of each powder is shown in Figure 6 and summarized in Table 10.

The D(10), D(50), and D(90) values refer respectively to the 10^{th}, 50^{th}, and 90^{th} quantile of the volume distribution of the powder, while the complete distribution is showed in Figure 6. The PSD of all six powders follows a log-normal distribution, which is the standard results from the atomization process. All powders show a distribution coherent with the ones expected for SLM and LMD processes.

The variability of the size distribution is described by the Span index, shown in the last column of Table 10. The Span index is calculated as:

$$\frac{D(90)-D(10)}{D(50)} \tag{2}$$

The larger the span, the larger the particle size distribution. There is no standard indicating the optimal value of span index, however, the literature provides some reference. For example, according to Tan et al. (2017) a span lower than 1.5 ensures a higher flowability.

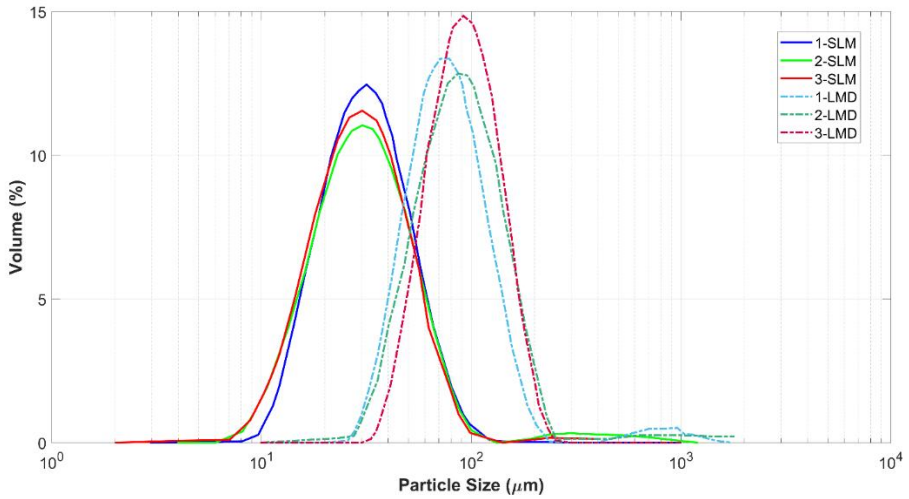

Fig 6. Particle size distribution of the powders used in this study.

Table 10. Quantiles of particle size distribution for all powders (µm).

Powder	D(10)	D(50)	D(90)	Span
1-SLM	17.0	31.0	57.6	1.31
2-SLM	15.3	30.5	61.4	1.51
3-SLM	15.3	29.8	56.5	1.38
1.LMD	44.6	76.9	140.9	1.25
2-LMD	48.7	87.9	158.4	1.25
3-LMD	56.1	93.3	153.9	1.05

The powder morphology in Figure 7 shows that all powders are composed of particles with an almost-spherical shape and the surfaces of larger particles are associated with satellite particles. Apparent density and flowability of the SLM and LMD powders are reported in Table 11; low flow time values indicate higher degrees of flowability. SLM powders have less flowability than LMD powders, and this is because attractive forces between particles increase as PSD decreases (Krantz et al., 2009). The apparent densities of the powders are similar, which was expected as their span values are comparable.

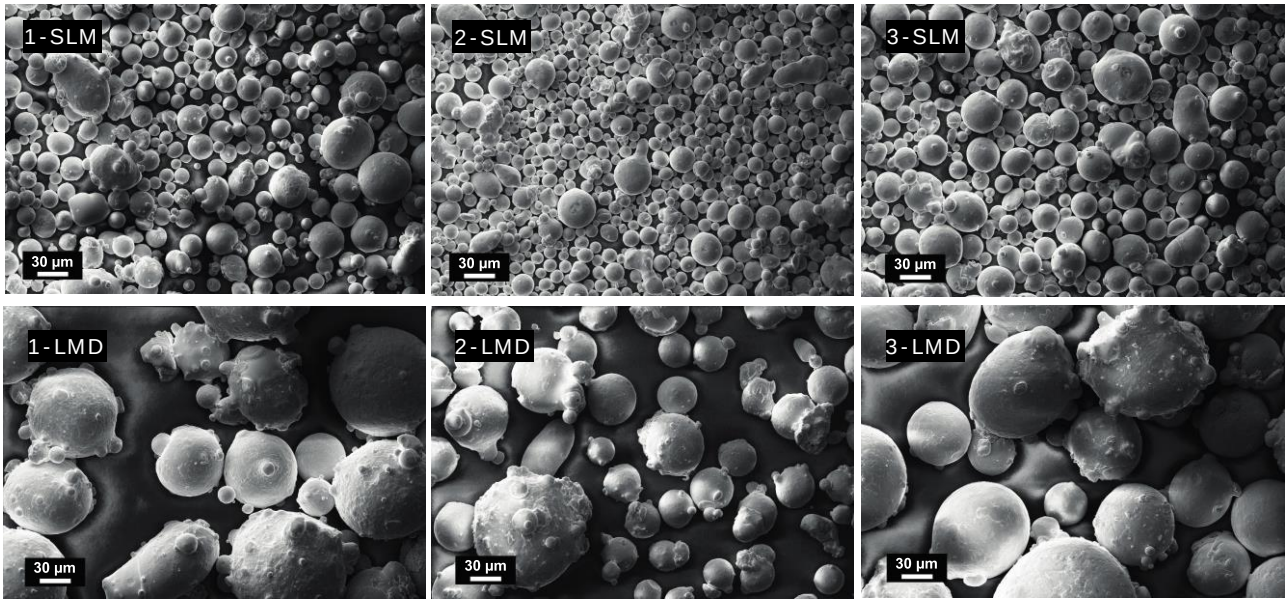

Fig 7. SEM images of powders used for SLM and LMD experiments.

Table 11. Apparent density and flowability of AISI 316L powders.

Powder	Apparent Density (kg/m^3)	Flow time (s)
1-SLM	4920	37
2-SLM	4880	40
3-SLM	4960	38
1.LMD	4850	18
2-LMD	4790	16
3-LMD	4900	15

Nitrogen and oxygen contents of the powders are shown in Table 12. Both recycled powders deviated greatly from the nominal composition of the standard AISI 316L batch (2-SLM and 3-SLM) .

Oxygen and nitrogen contents of the standard AISI 316L batch are much lower than those of powders produced using industrial recycled material. The presence of oxygen in stainless steel powders is believed to change the

wetting conditions of the melt pool, leading to balling on the solidified melt track. Balling reduces the quality of the solidified layer, leading to an increased porosity of the final 3D printed part, as indicated by Gu and Shen (2009) and Li et al. (2010). Si and Al contents were measured before sieving, and the results in Table 13 indicate that deoxidized powders have a much higher Al content than the standard material. The production of powders for AM applications starts from ingots with high chemical purity, which means low oxygen content and a controlled amount of alloying elements (for example N and Si). Powder batches 2 and 3 come from material produced in a steelmaking industry and the chemical composition is not as controlled as in the previous case, for this reason, the amount of alloying elements and oxygen is much higher in these two powders.

The high content of Si and Al was expected because these elements are the deoxidizing agents used to reduce the amount of oxygen in recycled steels. The presence of higher values of Si content might indicate that 2-SLM, 3-SLM, and 2-LMD and 3-LMD powder could not be properly processed, as showed by Engeli et al. (2016) and Kakinuma et al. (2016), respectively for SLM and LMD process. Nevertheless, we want to point out that these works used nickel-based superalloys and not stainless steel 316L. As a consequence, the feasibility of using non-standard stainless steel powders should be verified as the high Al, Si and O content could have an impact on the processability of the powders.

Table 12. Oxygen and nitrogen contents of AISI powders.

	1-SLM	2-SLM	3-SLM	1-LMD	2-LMD	3-LMD
O	90 ppm	170 ppm	150 ppm	150 ppm	140 ppm	150 ppm
N	50 ppm	370 ppm	250 ppm	29 ppm	320 ppm	210 ppm

Table 13. Si and Al contents of the three ingots of powder.

	Standard AISI 316L	**Industrial AISI 316L–Si**	**Industrial AISI 316L–Al**
Si	29 ppm	52 ppm	42 ppm
Al	300 ppm	3100 ppm	3500 ppm

3.2 SLM: Results and discussion

3.2.1 SLM: density of printed samples

Table 14 presents the densities of the 3D printed part made from all the samples at every parameter combination (treatment), as well as the standard deviations. Figure 8 shows the effect of energy density on the density of the 3D printed part for powders 2 and 3 (SLM).

Table 14. Densities of powders 2 and 3 (SLM process).

Powder 2 -SLM			Powder 3-SLM		
Treatment	**Density (g/cm^3)**	**St. dev**	**Treatment**	**Density (g/cm^3)**	**St. dev**
1	7.935; 7.943	0.006	1	7.957; 7.961	0.003
2	7.877; 7.860	0.012	2	7.865; 7.864	0.000
3	7.910; 7.918	0.005	3	7.926; 7.814	0.080
4	7.934; 7.921	0.009	4	7.963; 7.940	0.016
5	7.900; 7.903	0.002	5	7.950; 7.950	0.000
6	7.901; 7.897	0.002	6	7.889; 7.901	0.008
7	7.522; 7.523	0.001	7	7.636; 7.627	0.006
8	7.936; 7.914	0.016	8	7.958; 7.934	0.017
Renishaw	7.918; 7.930; 7.904; 7.926; 7.936; 7.928	0.011	Renishaw	7.960; 7.955; 7.952; 7.937; 7.949; 7.956	0.008

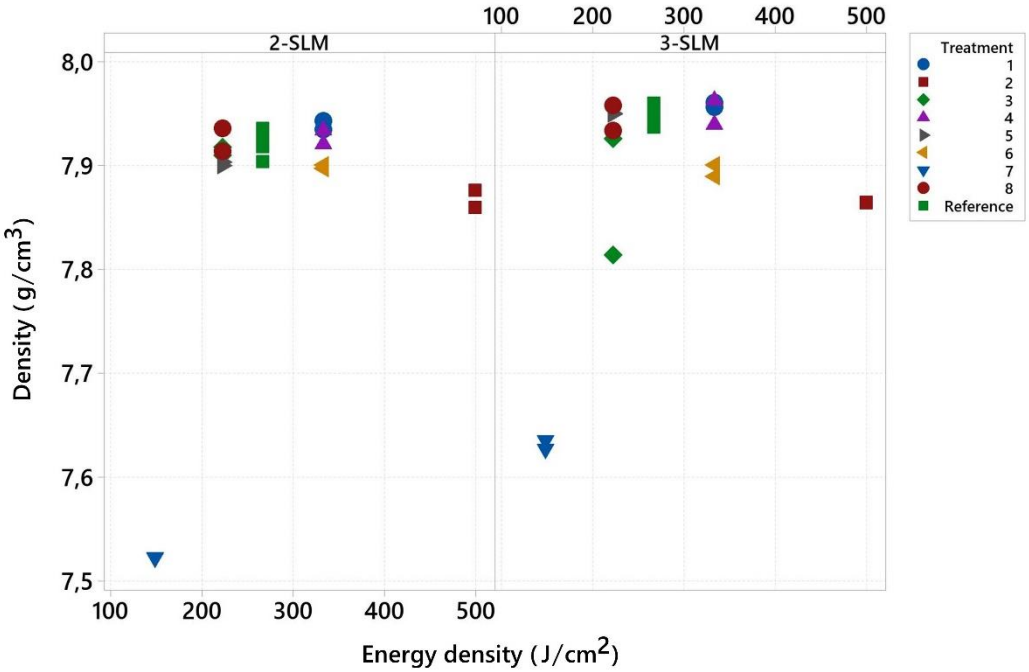

Fig 8. Printed part densities of the different treatments in response to energy

Part density varied between 7.52 and 7.94 g/cm^3 for powder 2-SLM, which accounts for 94.2%-99.5% of the nominal density of the material. For powder 3-SLM part density varied between 7.63-7.96 g/cm^3, accounting for 95.6%-99.74% of the nominal density of AISI 316L. The relationship between energy density and part density agrees with previous findings for both powders. For example, Cherry et al. (2015) showed that at low energy density values (Treatment 7), the laser tracks do not overlap due to the low temperature of the melt pool, resulting in the formation of large defects. In contrast, excessive energy density (Treatment 2) generates porosity due to the overheating of the melt pool. In the range of 222–333 J/cm^2, 3D printed part density remains higher than 99% of the reference value of AISI 316L. ANOVA of density data identified the best treatments for each powder. Based on the ANOVA, a Dunnett comparison test compared treatments 1, 3, 4, 5, 6 to the reference (Treatment 9). Treatments 7 and 2 were not included in the analysis because they do not belong to the feasibility region, as discussed previously.

Table 15. Powder 2-SLM ANOVA results for part density (Box Cox transformation was applied to the data)

Source	Df	SS	MS	F-value	P-value

Treatment	6	0.0026	0.0004	4.54	0,015
Error	11	0.0011	0.0000		
Total	17	0.0037			

The results of the statistical analysis show that some treatments differ in terms of final part density (Table 15). The Dunnet test identifies the treatments that differ significantly from the reference condition (Table 16).

Table 16. Dunnet test results (powder 2-SLM).

Treatment	**N**	**Mean**	**Grouping**
9 (Control)	6	7.924	A
1	2	7.939	A
4	2	7.928	A
8	2	7.925	A
3	2	7.914	A
5	2	7.902	A
6	2	7.899	

The Dunnet test indicates treatments 1, 3, 4, 5 and 8 result in the same part density as Treatment 9 for powder 2-SLM.

Similarly, statistical analysis on the different powders from 3-SLM (Treatments 2 and 7 were not included) indicate that some conditions produce 3D printed parts with significantly lower density than others, see Table 17.

Table 17. Powder 3-SLM ANOVA results for part density (Box Cox transformation was applied to the data)

Source	**Df**	**SS**	**MS**	**F-value**	**P-value**
Treatment	6	0.0067	0.0011	5.76	0.006
Error	11	0.0021	0.0002		
Total	17	0.0089			

Table 18. Dunnet test results (powder 3-SLM)

Treatment	**N**	**Mean**	**Grouping**

9 (Control)	6	7.952	A
1	2	7.958	A
4	2	7.953	A
5	2	7.950	A
8	2	7.947	A
3	2	7.899	
6	2	7.895	

The final part density of treatments 1, 4, 5 and 8 of the 3-SLM powders are not statistically different from the control treatment (Table 18). For both powders, there was no process treatment that produced statistically better results than the reference treatment, consequently, specimens made for tensile strength were built using Treatment 9.

The preliminary study on density verified the feasibility of printing recycled powder using the SLM process. The results showed that the process parameters for standard AISI 316L can be also used for the recycled powders, this means that the difference in the chemical composition reported in Section 3.1 is not significant. It is important to note that in SLM a proxy for the productivity of the process is proportional to the inverse of the Energy density. The possibility to use the same process parameters for standard and recycled material implies that the SLM productivity is not influenced by the type of powder used (standard or recycled), which is a strong advantage from an industrial point of view. In addition, the assumption that the higher O content of 2-SLM and 3-SLM could cause higher porosity was proved wrong as both powders reached density higher than 99%. The processability of the recycled powders is then verified.

3.2.2 SLM: tensile properties of printed samples

The optimal process parameters found in the preliminary analysis (Treatment 9 in Table 4) were used to produce tensile specimens according to the experimental plan described in Section 2.3.2.

Table 19 summarizes the tensile properties of AISI 316L specimens produced with SLM technology, along with literature values for comparison purposes. The literature values are from samples produced with standard AISI 316L powders.

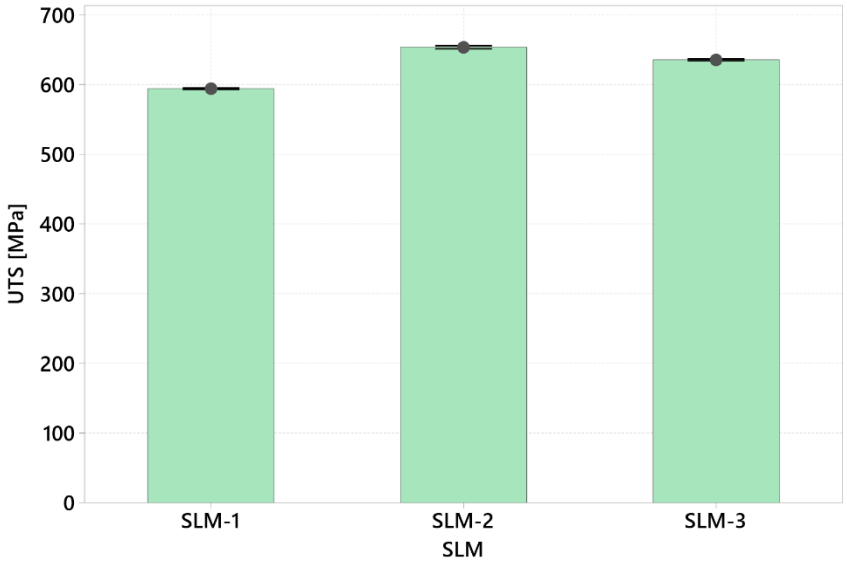

Fig 9. UTS values for the different powders.

Figure 9 shows that the three different powders yield products with different UTS values. Powders 2-SLM and 3-SLM powders result in higher UTS values than the standard powder (1-SLM). ANOVA indicates that the effect of powder on UTS is highly significant ($p = 0.00$). The relative increase in UTS in powder 2-SLM and 3-SLM is about 10% and 7% over 1-SLM, respectively. This improvement is not enough to conclude that recycled powders are more effective than the standard material.

Previous reports on the mechanical properties of standard AISI 316L produced by the SLM process show large variation, which depends on the number of samples produced, the machine type, and powder properties. Indeed, the tensile properties of material produced in the present work fit well with the previous findings. Yield strength shows a similar pattern as UTS for recycled powders 2-SLM and 3-SLM, thus, these values are also higher than those from standard AISI 316L. In contrast, the Young modulus and the elongation values are similar for all three powders.

Table 19. Summary of tensile properties of SLM powders (means ± standard deviation).

Paper	**Laser**	**Powder**	**UTS (± 1σ) [MPa]**	**YS (± 1σ) [MPa]**	**Young modulus (± 1σ) [GPa]**	**El (± 1σ) [%]**
This work	Pulsed	**1-SLM**	594 ±0.89	403.2 ±11.39	184 ± 10.13	58 ± 2.20
	Pulsed	**2-SLM**	653.8 ±1.79	470.8 ±9.36	189 ± 5.49	56 ± 2.23
	Pulsed	**3-SLM**	635.8 ±1.10	438.8 ±11.48	185 ± 6.44	57 ± 2.18
Lavery et al. (2017)	Pulsed	-	524	385	195.54 ±7.0	22
Mower and Long (2016)	Continuous	-	680-717	496-473	180–193	28–30
Carlton et al. (2016)	Continuous	-	540 ±120			44
Liu et al. (2015)	Continuous	-	664.7 ±17.5	488.9 ±16.7		29.3 ± 2.1
Liverani et al. (2017)	Continuous	-	550-600	450-500		40–70

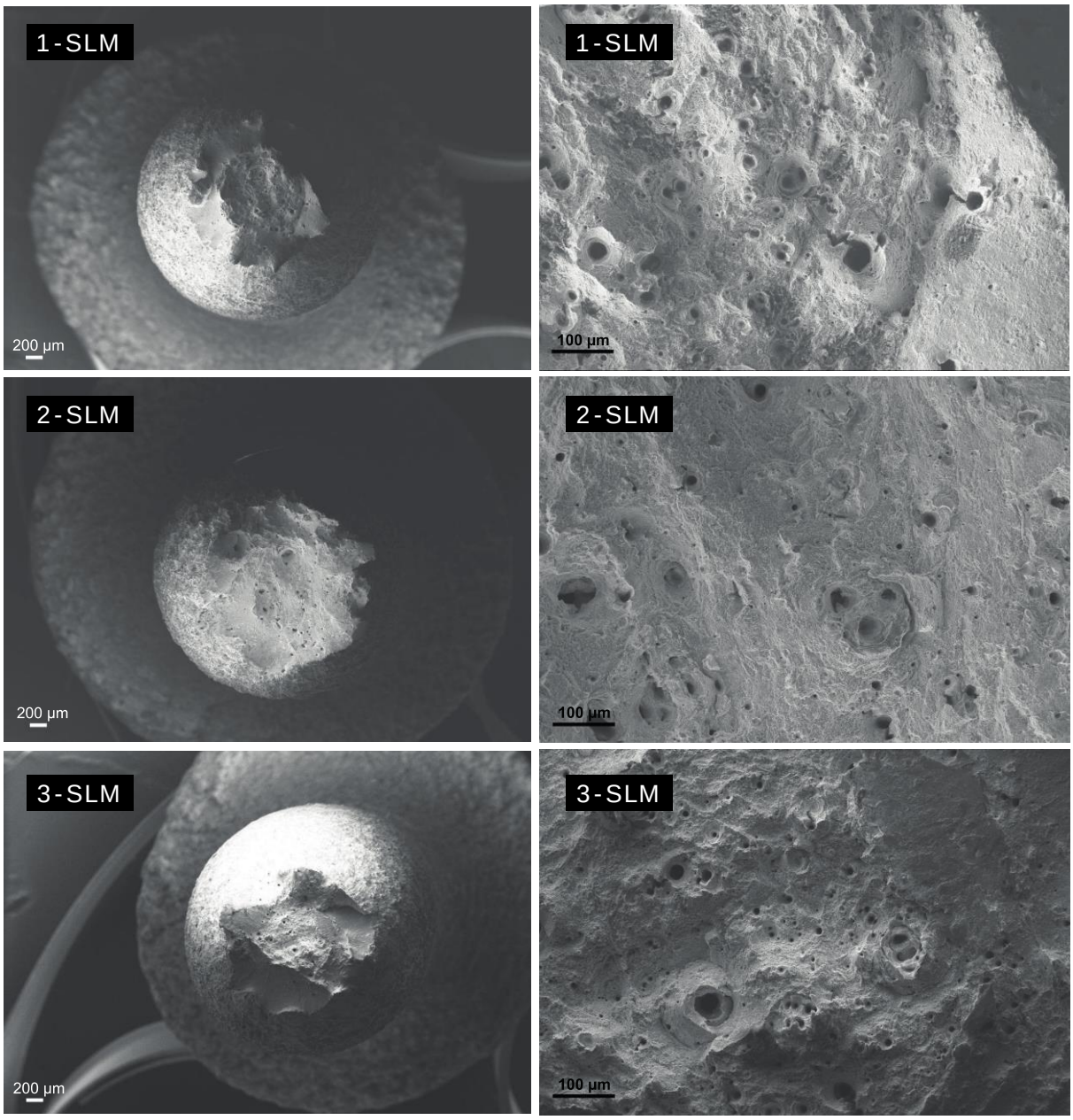

Fig 10. SEM images of fracture surfaces of specimens tested for tensile strength. Top to bottom rows: powder 1-SLM, powder 2-SLM, and powder 3-SLM.

A scanning electron microscope (SEM; EVO-50, Carl Zeiss, Germany) was used to analyse fractographic sections of the powders, (Figure 10). The samples show very similar microstructures, i.e., a fractured surface reveals ductile features as well as dimples across the section.

In conclusion, powders produced from recycled metal and then used in the SLM process have a similar solidification mechanism; and using optimal processing conditions, the recycled metal produced the same

processability as the reference powder material. The tensile properties of the products of recycled metal were comparable to the literature values and better than the standard powder (AISI 316L).

3.3 LMD: results and discussion

3.3.1 LMD: density of printed samples

The densities of all LMD samples are reported in Table 20 and the relationship between density and process parameters (power and powder flow rate) is shown in Figure 11.

Table 20. Densities of powders 2 and 3 (LMD process).

Density of powder 2-LMD		**Density of powder 3 - LMD**	
Treatment	**Density (g/cm^3)**	**Treatment**	**Density (g/cm^3)**
1	7.884	1	7.868
2	7.883	2	7.855
3	7.888	3	7.858
4	7.879	4	7.885
5	7.874	5	7.878
6	7.886	6	7.846
7	7.888	7	7.874
8	7.882	8	7.886
9	7.881	9	7.876

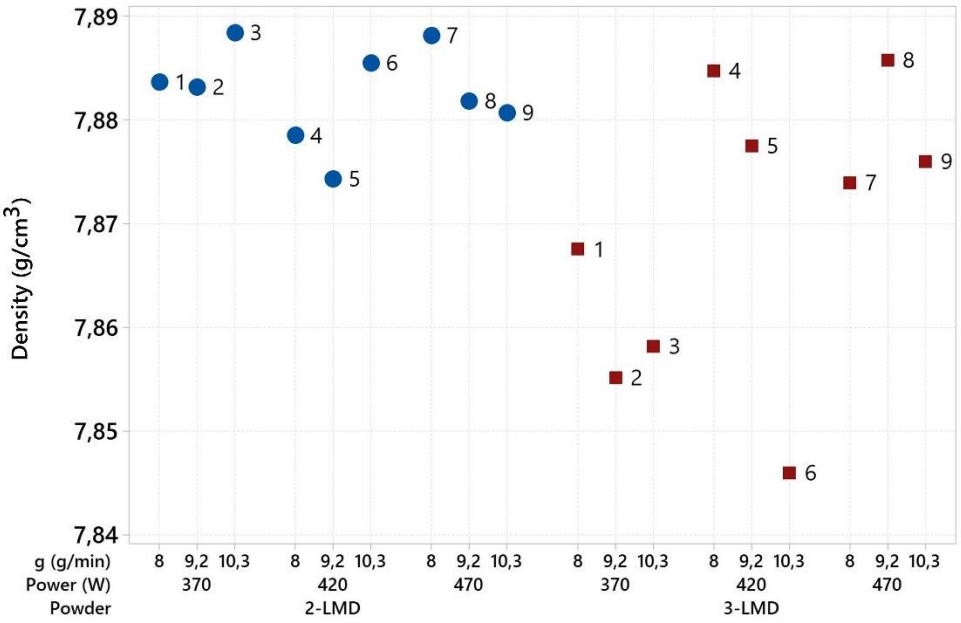

Figure 11. Densities of powders 2-LMD and 3-LMD under different treatments. Labels refer to the treatment number.

The printed part density varied between 7.874 and 7.888 g/cm^3 for 2-LMD and 7.846-7.886 g/cm^3 for 3-LMD, accounting for 98.7%-98.8% and 98.3%-98.8%, respectively, of the nominal density of the base material. The range of the parameters investigated for powder 2-LMD had no meaningful effect on 3D printed part density. In contrast, some conditions for powder 3-LMD produced insufficient 3D printed part density. All samples failed to reach a high density at low power. At 420 W and 10.3 g/min, the sample had an unexpected low density. Samples from product of powder 3-LMD and treatment 6 were analysed because of their low part density. The samples were cut and polished, and the cross-section revealed defects on the surface.

The quantity of powder available for the LMD process was insufficient to carry out extensive experiments. Experiments were not replicated. Consequently, it is not possible to perform ANOVA and the Dunnet test. However, using a Bonferroni approach, we determined that the powder does not influence part density

In conclusion, we were unable to determine the influence of process parameters (power and powder flow rate) of recycled powder on final printed part density. ANOVA results without replicates found no difference between the treatments. Therefore, we selected the centre point (i.e. the reference condition in Table 18), which is also the combination used for the standard AISI316L powder (1-LMD). The recycled powder was successfully processed using the same process parameters used for the standard powder. Therefore, despite the

differences in chemical composition, the processability of recycled powders is the same as the standard material.

3.3.2 LMD: tensile properties of printed samples

The tensile properties of the AISI 316L specimen produced with LMD technology are summarized in Table 21. The table includes literature values using standard AISI 316L powders.

Table 21. Summary of tensile properties of LMD powders

Paper	**Powder**	**UTS (± 1σ) [MPa]**	**YS (± 1σ) [MPa]**	**Young modulus (± 1σ) [GPa]**	**El (± 1σ) [%]**
This work	1-LMD	585.5 (±3.1)	412.5 (±6.2)	179 (±5.7)	54 (±6.8)
	2-LMD	675.0 (±2)	511.7 (±7.6)	179 (±4.1)	49 (±4.9)
	3-LMD	630.0 (±1.4)	457.5 (±6.4)	184 (±1.3)	54 (±0.0)
Yu et al. (2013)		≈650	≈490		≈50
Ziętala et al (2016)		703	479		46
Zhang et al. (2014)		536	352		46
Yadollahi et al. (2015)		620–660	405–415		34–40

Figure 12 shows that 2-LMD and 3-LMD powders have higher UTS values compared to the standard powder (1-LMD). ANOVA indicates that the powders have a highly significant ($p = 0.00$) effect on the UTS.

Powder 2-LMD showed an increase in UTS of 15% compared to powder 1-LMD, while 3-LMD increased the UTS of 8% compared to 1-LMD. As for SLM, these improvements are not enough to conclude that recycled powders have higher performances than the standard material.

Therefore, the results demonstrate that, at the least, the two recycled powders are as effective as the standard material in terms of mechanical static performance. The results of the LMD experiments are comparable to those of the SLM process, i.e., recycled powder increases the UTS, and powder 2-LMD (deoxidized with Si) performs the best. The YS trend is similar to that of UTS, while elongation and Young modulus did not vary

with the powder. These results are all consistent with the SLM results. Moreover, the tensile properties are comparable to literature values on AISI 316L.

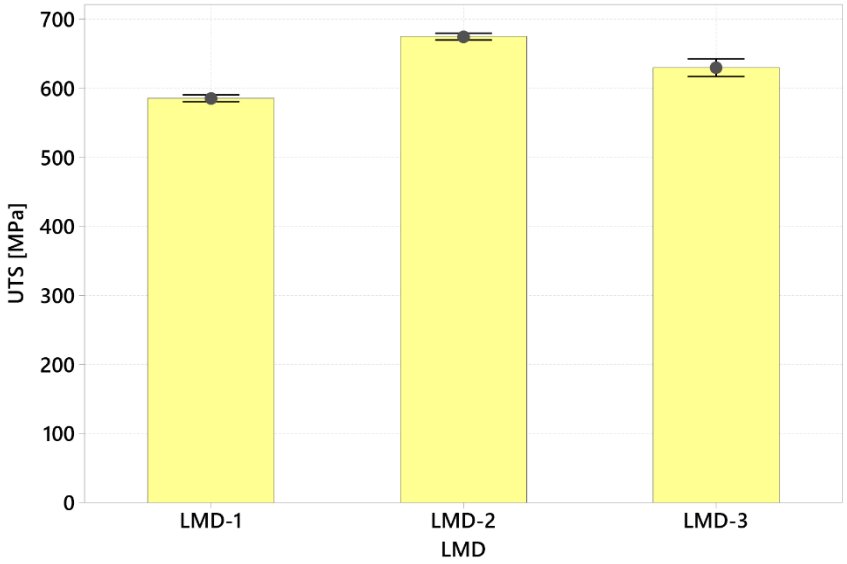

Fig 12. UTS values of LMD powders

The fracture sections in Figure 13 show ductile fracture features as well as dimples across the section. Overall, the LMD powders produced using recycled material have promising mechanical properties. These properties and the processability of LMD powders are comparable with those of the standard powder (AISI 316L) and with literature values.

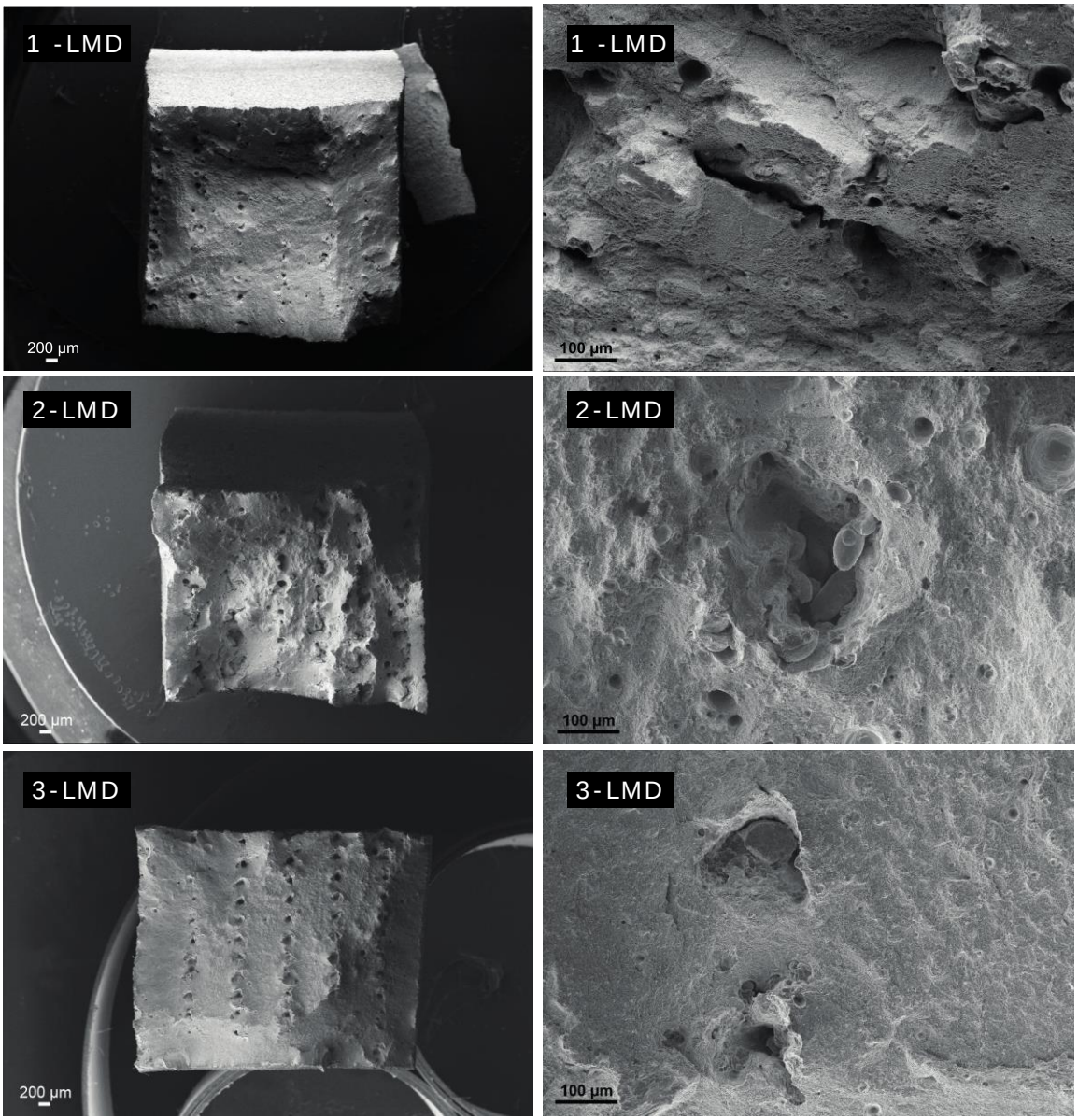

Figure 13. SEM images of fracture surfaces of specimens tested for tensile strength under two magnifications. Top to bottom rows: powder 1-LMD, powder 2-LMD, and powder 3-LMD

4- Discussion

Powders from recycled AISI 316L were atomized using a pilot VIGA plant and then used to produce parts using two additive manufacturing technologies, SLM and LMD. They showed deviations in terms of chemical composition from the standard material, AISI 316L and as expected, the O, Si, and Al contents varied among the three batches. The high amount of Si and Al did not result in a lack of processability. The preliminary analysis showed that the process parameters optimized for the standard material could also be used for the recycled material, and this is true for both SLM and LMD processes. Process parameters in SLM and LMD

are closely related to the productivity of the process, and we concluded that recycled powders can be processed without having an impact on the speed and cost of the additive process. This indicates that the two processes are highly robust, as they can successfully produce high-density materials using powders with industrial chemical compositions.

The increased amount of Si and Al did not impact on the tensile properties. The rankings of powders in terms of UTS and YS are the same for LMD and SLM, indicating that the two processes are consistent. The tensile results showed a small increase (around 7-10% for SLM, 8-15% for LMD) in terms of strength for the recycled powders. This improvement is not enough to state that powder batches AISI-Si and AISI-Al increase the performances of stainless steel 3D parts, a more extensive experimental campaign is needed to focus on the subject and to study also other properties, such as fatigue. We can conclude that using recycled material to produce powders does not reduce the tensile properties of AISI 316L.

From a technological point of view, it is possible to compare LMD and SLM results as both processes were run using the same powders. Compared to the work in literature, we used powders produced from the same atomization campaign and therefore we do not have the influence of the powder batch on the tensile results. The results showed that there is no difference in terms of mechanical properties between SLM and LMD. The recycled powders and the standard material have comparable elongation after fracture and Young modulus values. The variability of the tensile properties of the recycled powders is comparable with the one of the standard powder, ensuring ì high replicability of the results.

The environmental implications of these results are twofold. Firstly, the use of recycled material to produce metal powders for SLM and LMD has been verified with the production of 3D parts, such as tensile specimens. Secondly, this study showed that to reduce the environmental impact of AM one should not only focus on the processes itself, but it is possible to look at the overall supply chain. And in this case, the atomization process was the key. At present, the industrial practice in terms of sustainability considers only the reuse of the metal powder which is not melted during the process (especially in SLM). However, in this study we showed that it is possible to apply a wider approach to the sustainability of AM processes.

It is important to know that to produce powders from recycled material, the atomization process did not require any additional set-up or change in the process parameters. Therefore, there are no hidden costs or environmental trade-off which could reduce, or even cancel, the advantages of using the recycle material.
Eventually, the last aspect worth commenting is the cost reduction. Using recycled metal will reduce the costs for powder supply. Cost is still considered one of the main disadvantages of AM technology; however, using scrap metal will decrease production costs of 3D metal parts. Moreover, the results of this work also indicate that it is not necessary to use powders of high purity to obtain good mechanical properties; and the feasibility window of process parameters does not change with slight modifications in the chemical composition of the feedstock.

5 Conclusion

The objective of the investigation was to evaluate the feasibility of using the recycled powders in AM processes. The recycled and standard powders were characterized in terms of particle size distribution, shape, and chemical composition., for this reason a preliminary analysis covering the ability to produce samples with high density was carried out. Tensile specimens were successfully printed using the standard process parameters and the mechanical properties are coherent with the expected strength and elongation.

The environmental sustainability of AM is being questioned, due the high energy costs, material toxicity and waste production. The present experimental campaign showed that it is possible to produce powders for SLM and LMD processes using recycled material at the atomization stage. This result shows that the reduction of the environmental impact of AM technologies should not focus only on the process itself but also use a wider approach and consider the overall supply chain.

In conclusion, the potential of recycled materials to produce metal powders for additive manufacturing has been verified. In addition, using recycled metal will reduce the costs for powder supply.

Further studies will be focused on:

1. Testing different metal alloys produced from recycled material, for example nickel-based superalloys and Maraging steel.

2. Studying the different deterioration behaviour for recycled powders compared to standard AM powder in terms of flowability, chemical composition, and particle shape. This investigation will include the important topic of sustainability in the recycling of metal powder for AM processes.
3. Investigating fatigue performance of printed samples using the recycled powders.

Acknowledgments

The authors would like to acknowledge GF Machining Solution S.p.A. for their assistance in machining the LMD tensile specimens by using EDM.

Funding

This work was supported by Regione Lombardia under Project Made4Lo - Metal Additive for Lombardy (POR FESR 2014-2020).

References

Baumers, M., Beltrametti, L., Gasparre, A., Hague, R., 2017. Informing additive manufacturing technology adoption: total cost and the impact of capacity utilisation. Int. J. Prod. Res. 55(23), 6957–6970. https://doi.org/10.1080/00207543.2017.1334978

Carlton, H. D., Haboub, A., Gallegos, G. F., Parkinson, D. Y., MacDowell, A. A., 2016. Damage evolution and failure mechanisms in additively manufactured stainless steel. Mat. Sci. Eng. A. 651, 406–414. https://doi.org/10.1016/j.msea.2015.10.073

Chen, D., Heyer, S., Ibbotson, S., Salonitis, K., Steingrímsson, J. G., Thiede, S., 2015. Direct digital manufacturing: definition, evolution, and sustainability implications. J. Clean. Prod. 107, 615–625. https://doi.org/10.1016/j.jclepro.2015.05.009

Cherry, J. A., Davies, H. M., Mehmood, S., Lavery, N. P., Brown, S. G. R., Sienz, J., 2015. Investigation into the effect of process parameters on microstructural and physical properties of 316L stainless steel parts by selective laser melting. Int. J. Adv. Manuf. Tech. 76(5), 869–879. https://doi.org/10.1007/s00170-014-6297-2

Cooke, A., Slotwinski, J., 2012. Properties of metal powders for additive manufacturing: a review of the state of the art of metal powder property testing. US Department of Commerce, National Institute of Standards and Technology. http://dx.doi.org/10.6028/NIST.IR.7873

Demir, A.G, Colombo, P., Previtali, B., 2017. From pulsed to continuous wave emission in SLM with contemporary fibre laser sources: effect of temporal and spatial pulse overlap in part quality. Int. J. Adv. Manuf. Tech. 91(5), 2701–2714. https://doi.org/10.1007/s00170-016-9948-7

Engeli, R., Etter, T., Hoevel, S., Wegener, K., 2016. Processability of different IN738LC powder batches by selective laser melting. J. Mater. Process. Technol. 229, 484–491. https://doi.org/10.1016/j.jmatprotec.2015.09.046

Ford, S., Despeisse, M., 2016. Additive manufacturing and sustainability: an exploratory study of the advantages and challenges. J. Clean. Prod. 137, 1573–1587. https://doi.org/10.1016/j.jclepro.2016.04.150

Fullenwider, B., Kiani, P., Schoenung, J. M., Ma, K., 2019. Two-stage ball milling of recycled machining chips to create an alternative feedstock powder for metal additive manufacturing. Powder Technol. 342, 562–571. https://doi.org/10.1016/j.powtec.2018.10.023

Gu, D., Shen, Y., 2009. Balling phenomena in direct laser sintering of stainless steel powder: Metallurgical mechanisms and control methods. Mater. Des. 30(8), 2903–2910. https://doi.org/10.1016/j.matdes.2009.01.013

Huang, S. H., Liu, P., Mokasdar, A., Hou, L., 2013. Additive manufacturing and its societal impact: a literature review. Int. J. Adv. Manuf. Tech. 67(5), 1191–1203. https://doi.org/10.1007/s00170-012-4558-5

Kakinuma, Y., Mori, M., Oda, Y., Mori, T., Kashihara, M., Hansel, A., Fujishima, M., 2016. Influence of metal powder characteristics on product quality with directed energy deposition of Inconel 625. CIRP Annals, 65(1), 209–212. https://doi.org/10.1016/j.cirp.2016.04.058

Khayat, Z. R., Palmer, T. A., 2018. Impact of iron composition on the properties of an additively manufactured solid solution strengthened nickel base alloy. Mat. Sci. Eng. A. 718, 123–134. https://doi.org/10.1016/j.msea.2018.01.112

Krantz, M., Zhang, H., Zhu J., 2009. Characterization of powder flow: Static and dynamic testing. Powder Technol. 194, no. 3, 239–245. https://doi.org/10.1016/j.powtec.2009.05.001

Lavery, N. P., J. Cherry, S. Mehmood, H. Davies, B. Girling, E. Sackett, S. G. R. Brown, J. Sienz., 2017. Effects of hot isostatic pressing on the elastic modulus and tensile properties of 316L parts made by powder bed laser fusion. Mat. Sci. Eng. A. 693, 186–213. https://doi.org/10.1016/j.msea.2017.03.100

Li, R., Shi, Y., Wang, Z., Wang, L., Liu, J., Jiang, W., 2010. Densification behavior of gas and water atomized 316L stainless steel powder during selective laser melting. Appl. Surf. Sci. 256(13), 4350–4356. https://doi.org/10.1016/j.apsusc.2010.02.030

Lindemann, C., Jahnke, U., Moi, M., Koch, R., 2012. Analyzing product lifecycle costs for a better understanding of cost drivers in additive manufacturing. in 23rd Annual International Solid Freeform Fabrication Symposium–An Additive Manufacturing Conference. Austin Texas, USA.

Liu, Y., Yang, Y., Mai, S., Wang, D., Song, C., 2015. Investigation into spatter behavior during selective laser melting of AISI 316L stainless steel powder. Mater. Des. 87, 797–806. https://doi.org/10.1016/j.matdes.2015.08.086

Liverani, E., Toschi, S., Ceschini, L., Fortunato, A., 2017. Effect of selective laser melting (SLM) process parameters on microstructure and mechanical properties of 316L austenitic stainless steel. J. Mater. Process. Technol. 249, 255–263. https://doi.org/10.1016/j.jmatprotec.2017.05.042

Montgomery, D. C., 2017. Design and analysis of experiments, ninth ed. John Wiley & Sons, New Jersey.

Mower, T. M. Long, M.J., 2016. Mechanical behavior of additive manufactured, powder-bed laser-fused materials. Mat. Sci. Eng. A. 651, 198–213. https://doi.org/10.1016/j.msea.2015.10.068

Niaki, M. K., Torabi, S. A., Nonino, F., 2019. Why manufacturers adopt additive manufacturing technologies: The role of sustainability. J. Clean. Prod. 222, 381–392. https://doi.org/10.1016/j.jclepro.2019.03.019

Popovich, A., Sufiiarov, V., 2016. Metal Powder Additive Manufacturing, in: New Trends in 3D Printing. IntechOpen, pp. 215-236. http://dx.doi.org/10.5772/63337

Rejeski, D., Zhao, F., Huang, Y., 2018. Research needs and recommendations on environmental implications of additive manufacturing. Addit. Manuf. 19, 21–28. https://doi.org/10.1016/j.addma.2017.10.019

Sames, W. J., List, F. A., Pannala, S., Dehoff, R. R., Babu, S. S., 2016. The metallurgy and processing science of metal additive manufacturing. Int. Mater. Rev. 61(5), 315–360. https://doi.org/10.1080/09506608.2015.1116649

Sreenivasan, R., Goel, A., Bourell, D. L., 2010. Sustainability issues in laser-based additive manufacturing. Phys. Procedia. 5, 81–90. https://doi.org/10.1016/j.phpro.2010.08.124

Tan, J.H., Wong, W.L.E. and Dalgarno, K.W., 2017. An overview of powder granulometry on feedstock and part performance in the selective laser melting process. Add. Manuf. 18, 228–255. https://doi.org/10.1016/j.addma.2017.10.011

Tofail, S. A., Koumoulos, E. P., Bandyopadhyay, A., Bose, S., O'Donoghue, L., & Charitidis, C., 2018. Additive manufacturing: scientific and technological challenges, market uptake and opportunities. Mat. To., 21(1), 22-37. https://doi.org/10.1016/j.mattod.2017.07.001

Tomus, D., Rometsch, P. A., Heilmaier, M., Wu, X., 2017. Effect of minor alloying elements on crack-formation characteristics of Hastelloy-X manufactured by selective laser melting. Add. Manuf. 16, 65–72. https://doi.org/10.1016/j.addma.2017.05.006

Vock, S., Klöden, B., Kirchner, A., Weißgärber, T., Kieback, B., 2019. Powders for powder bed fusion: a review. Progr. Add. Manuf. 1–15. https://doi.org/10.1007/s40964-019-00078-6

Yadollahi, A., Shamsaei, N., Thompson, S. M., Seely, D. W., 2015. Effects of process time interval and heat treatment on the mechanical and microstructural properties of direct laser deposited 316L stainless steel. Mat. Sci. Eng. A. 644, 171–183. https://doi.org/10.1016/j.msea.2015.07.056

Yu, J., Rombouts, M., Maes, G., 2013. Cracking behavior and mechanical properties of austenitic stainless steel parts produced by laser metal deposition. Mater. Des. 45, 228–235. https://doi.org/10.1016/j.matdes.2012.08.078

Zhang, K., Wang, S., Liu, W., Shang, X., 2014. Characterization of stainless steel parts by laser metal deposition shaping. Mater. Des. 55, 104–119. https://doi.org/10.1016/j.matdes.2013.09.006

Ziętala, M., Durejko, T., Polański, M., Kunce, I., Płociński, T., Zieliński, W., Łazińska, M., Stępniowski, W., Czujko, T., Kurzydłowski, K.J., Bojar, Z., 2016. The microstructure, mechanical properties and corrosion resistance of 316 L stainless steel fabricated using laser engineered net shaping. Mat. Sci. Eng. A. 677, 1–10. https://doi.org/10.1016/j.msea.2016.09.028